A Conservative Local Discontinuous Galerkin Method for the Schrödinger-KdV System

Yinhua Xia[1],[*] and Yan Xu[1]

[1] *School of Mathematical Sciences, University of Science and Technology of China, Hefei, Anhui 230026, P.R. China.*

Abstract. In this paper we develop a conservative local discontinuous Galerkin (LDG) method for the Schrödinger-Korteweg-de Vries (Sch-KdV) system, which arises in various physical contexts as a model for the interaction of long and short nonlinear waves. Conservative quantities in the discrete version of the number of plasmons, energy of the oscillations and the number of particles are proved for the LDG scheme of the Sch-KdV system. Semi-implicit time discretization is adopted to relax the time step constraint from the high order spatial derivatives. Numerical results for accuracy tests of stationary traveling soliton, and the collision of solitons are shown. Numerical experiments illustrate the accuracy and capability of the method.

1 Introduction

We consider the long wave and short wave interaction system

$$i(u_t + c_1 u_x) + \delta_1 u_{xx} = \alpha u v, \tag{1.1a}$$

$$v_t + c_2 v_x + \delta_2 v_{xxx} + \gamma(v^2)_x = \beta(|u|^2)_x, \tag{1.1b}$$

where u is a complex-valued function of real variables x and t, v is a real-valued function of x and t, and constants c_i, δ_i, α, β, γ are real. The Sch-KdV system arises in various physics contexts as a model for interaction of long and short nonlinear waves. For example, Kawahara et al. [13] derived the system as a model for the interaction between long gravity waves and capillary waves on the surface of shallow water. In [2, 14, 15],

---

[*]Corresponding author. *Email addresses:* `yhxia@ustc.edu.cn` (Y. Xia), `yxu@ustc.edu.cn` (Y. Xu)

the system is derived for resonant ion-sound/Langmuir-wave interactions in plasmas. Similarly, one can obtain the system as the unidirectional reduction of a model for the resonant interaction of acoustic and optical modes in a diatomic lattice [21]. In this system, the short wave is usually described by the Schrödinger type equation and the long wave is described by the wave equation accompanied with a dispersive term. When the resonance condition $c_1 = c_2$ holds, this system is known as the coupled Schrödinger-Korteweg-de Vries (Sch-KdV) system. Finite element methods and meshless methods have been considered in [3,4,12].

If $\delta_2 \neq 0$, then by using the suitable transformation in [1,2], the Sch-KdV system (1.1) is reduced to

$$iu_t + \frac{3}{2}u_{xx} = \frac{1}{2}uv, \tag{1.2a}$$

$$v_t + \frac{1}{2}v_{xxx} + \frac{1}{2}(v^2)_x = -\frac{1}{2}(|u|^2)_x. \tag{1.2b}$$

We will also have occasion to consider the case when $\delta_2 = \gamma = 0$ in (1.1). In this case, the system (1.1) is reduced to the form

$$iu_t + u_{xx} = uv, \tag{1.3a}$$

$$v_t = -(|u|^2)_x. \tag{1.3b}$$

This system has independent mathematical interest because it has been shown to be a completely integrable structure [5].

In this paper, we will present the conservative local discontinuous Galerkin (LDG) scheme for the system (1.2) and (1.3). For the general system (1.1), the LDG scheme is similar to these two special cases. Conservative quantities of the number of plasmons, energy of the oscillations and the number of particles in discrete versions are preserved in the LDG scheme for the Sch-KdV system. The conservative scheme for Sch-KdV system is very crucial for the long time simulation, especially for the integrable system (1.3).

The discontinuous Galerkin (DG) method is a class of finite element methods, using discontinuous, piecewise polynomials as the solution and the test spaces. It was first designed as a method for solving hyperbolic conservative quantities containing only the first order spatial derivatives, e.g. Reed and Hill [16] for solving linear equations, and Cockburn et al. [7–10] for solving nonlinear equations. The LDG method is an extension of the discontinuous Galerkin method aimed at solving partial differential equations (PDEs) containing higher than first order spatial derivatives. The idea of the LDG method is to rewrite the equations with higher order derivatives into a first order system, then apply the DG method on the system. The design of the numerical fluxes is the key ingredient to ensure stability. The LDG methods for a general KdV type equation with third order derivatives [22] and general Schrödinger equation [19] have been designed, in which the dissipation mechanism were introduced in the scheme. Recently, a conservative DG method is proposed in [6], in which the conservation properties are numerically

shown to impart the approximations with beneficial attributes. Also, the LDG scheme for another kind of long and short waves interaction equation Zakharov system has been proposed in [18], which is a Schrödinger equation coupled with a wave equation. For a detailed description about the LDG methods for high-order time-dependent PDEs, we refer the readers to [20].

This paper is organized as follows. In Section 2, we review the conservative quantities of the Sch-KdV system, and then develop the LDG scheme for the system. The conservation properties of the LDG method are also proved. In Section 3, we perform numerical experiments to show the accuracy and capability of the scheme, including accuracy tests of stationary traveling soliton, and the collision of coupled and single solitons. Concluding remarks are given in Section 4.

2   The LDG method for the Sch-KdV system

In this section, we will develop and analyze the LDG method for the system (1.2) with an initial condition

$$u(x,0) = u_0(x)$$

and the periodic or homogeneous Dirichlet boundary condition in the domain Ω.

2.1   Conservative quantities of the Sch-KdV system

It can be easily verified that the system (1.2) has the following conservative quantities [2]:

- The number of plasmons,

$$I_1 = \int |u|^2 dx.$$

- The momentum of the oscillations,

$$I_2 = \int (v^2 + \mathrm{i}(u\bar{u}_x - \bar{u}u_x))dx,$$

  where $\bar{u}$ denotes the conjugate of u.

- The energy of the oscillations

$$I_3 = \int \left(3|u_x|^2 + v|u^2| + \frac{1}{3}v^3 - \frac{1}{2}(v_x)^2 \right).$$

- The number of particles

$$I_4 = \int v dx.$$

We will give the proof of the above conservative quantities in the discrete version for the LDG method of the Sch-KdV system.

2.2   Notations and finite element space for the LDG method

Let $\mathcal{T}_h$ be a partition of Ω with shape-regular elements K. Let Γ denote the union of the boundary faces of elements $K \in \mathcal{T}_h$, i.e. $\Gamma = \cup_{K \in \mathcal{T}_h} \partial K$, and $\Gamma_0 = \Gamma \backslash \partial \Omega$. In order to describe the flux functions we need to introduce some notations. We denote the mesh by $K_j = [x_{j-\frac{1}{2}}, x_{j+\frac{1}{2}}]$, for $j = 1, \cdots, N$. The center of the cell is $x_j = (x_{j-\frac{1}{2}} + x_{j+\frac{1}{2}})/2$ and $h_j = x_{j+\frac{1}{2}} - x_{j-\frac{1}{2}}$, $h = \max_j h_j$. And $u_{j+\frac{1}{2}}$ denote the value of function u at $x_{j+\frac{1}{2}}$. If u is a function on K_j and K_{j+1}, but possibly discontinuous across cell interface $x_{j+\frac{1}{2}}$, let $u_{j+\frac{1}{2}}^+$ and $u_{j+\frac{1}{2}}^-$ denote the value of u at $x_{j+\frac{1}{2}}$, from the right cell, K_{j+1}, and from the left cell, K_j, the left and right trace, respectively.

We will use the notations

$$(f,g)_K := \int_K f(x)\bar{g}(x)dx,$$

$$<f,g>_{\partial K_j} := (f\bar{g})_{j+\frac{1}{2}}^+ + (f\bar{g})_{j-\frac{1}{2}}^-,$$

$$(f,g)_h := \sum_{K \in \mathcal{T}_h} (f,g)_K,$$

$$<f,g>_h := \sum_{K \in \mathcal{T}_h} <f,g>_{\partial K},$$

where $\bar{f}, \bar{g}$ denotes the conjugate of functions f, g.

Let $\mathcal{P}_r^k(K)$ and $\mathcal{P}_c^k(K)$ be the space of real and complex polynomials of degree at most $k \geq 0$ on $K \in \mathcal{T}_h$ respectively. The finite element spaces are denoted by

$$V_h^r := \{\phi \in L_r^2(\Omega) : \phi|_K \in P_r^k(K), \forall K \in \mathcal{T}_h\}, \tag{2.1}$$

$$V_h^c := \{\psi \in L_c^2(\Omega) : \psi|_K \in P_c^k(K), \forall K \in \mathcal{T}_h\}, \tag{2.2}$$

with the tessellation $\mathcal{T}_h$ of the computational domain Ω. Note that functions in V_h^r and V_h^c are allowed to be completely discontinuous across element interfaces.

2.3   The LDG method of the Sch-KdV system

To construct the LDG method, firstly we rewrite the generalized Sch-KdV system (1.2) as a system containing only first order derivatives:

$$iu_t + \frac{3}{2}m_x - \frac{1}{2}uv = 0, \tag{2.3a}$$

$$m = u_x, \quad v_t + \frac{1}{2}(p+q+s)_x = 0, \tag{2.3b}$$

$$w = v_x, \quad p = w_x, \tag{2.3c}$$

where $s = |u|^2$ and $q = v^2$.

To simplify the notations, we still use u, m, v, w and p to denote the numerical solutions. Then, we define the LDG method for the Sch-KdV system (2.3): Find $u,m \in V_h^c$, $v,w,p,q,s \in V_h^r$, such that

$$i(u_t,\phi)_K + \frac{3}{2} <\hat{m}\boldsymbol{v},\phi>_{\partial K} - \frac{3}{2}(m,\phi_x)_K - \frac{1}{2}(uv,\phi)_K = 0, \tag{2.4a}$$

$$(m,\eta)_K = <\hat{u}\boldsymbol{v},\eta>_{\partial K} - (u,\eta_x)_K, \tag{2.4b}$$

$$(v_t,\psi)_K + \frac{1}{2} <(\hat{p}+\hat{q}+\hat{s})\boldsymbol{v},\psi>_{\partial K} - \frac{1}{2}(p+q+s,\psi_x)_K = 0, \tag{2.4c}$$

$$(w,\xi)_K = <\hat{v}\boldsymbol{v},\xi>_{\partial K} - (v,\xi_x)_K, \tag{2.4d}$$

$$(p,\zeta)_K = <\hat{w}\boldsymbol{v},\zeta>_{\partial K} - (w,\zeta_x)_K, \tag{2.4e}$$

for all test function $\psi,\eta \in V_h^c$ and $\psi,\xi,\zeta \in V_h^r$, for all elements $K \in \mathcal{T}_h$, where

$$(s,\psi)_K = (|u|^2,\psi)_K, \quad \forall \psi \in V_h^r, \tag{2.5}$$

$$(q,\psi)_K = (v^2,\psi)_K, \quad \forall \psi \in V_h^r, \tag{2.6}$$

and $\boldsymbol{v}$ is the unit normal vector of the element K. The "hat" terms $\hat{u},\hat{m},\hat{w},\hat{v},\hat{p},\hat{q},\hat{s}$ in (2.4) in the cell boundary terms from integration by parts are the so-called "numerical fluxes", which are functions defined on the edges and should be designed based on the different guiding principles for the different PDEs to ensure stability and local solvability of the intermediate variables w, p and m.

In the following procedure of proving the discrete conservative quantities, it turns out that we can take the simple choices of numerical fluxes as

$$\hat{p} = \frac{1}{2}(p^- + p^+), \quad \hat{q} = \frac{1}{2}(q^- + q^+), \quad \hat{s} = \frac{1}{2}(s^- + s^+), \tag{2.7a}$$

$$\hat{u} = u^-, \quad \hat{m} = m^+, \quad \hat{w} = w^-, \quad \hat{v} = v^+. \tag{2.7b}$$

The choice for the fluxes (2.7a) is not unique. Considering the compactness of the stencil and the optimal accuracy, the crucial part is taking $\hat{u}$ and $\hat{m}$ from opposite sides and $\hat{w}$ and $\hat{v}$ from opposite sides. Unlike the LDG scheme for the KdV equation [22], here we use the average numerical fluxes for $\hat{p},\hat{q}$ and $\hat{s}$ which is crucial to preserve the conservation of the scheme.

2.4 Conservation properties of the LDG method

We will give the proof of the discrete conservative quantities in the following.

Proposition 2.1. (Discrete conservative quantities) The solution to the LDG method (2.4) and (2.7a) possesses the discrete conservative quantities as

- the number of plasmons: $I_{h,1} = \int |u|^2 dx$,

- the energy of the oscillations: $I_{h,3} = \int (3|m|^2 + v|u|^2 + \frac{1}{3}v^3 - \frac{1}{2}(w)^2)$,

- the number of particles $I_{h,4} = \int v dx$,

with periodic or homogeneous Dirichlet boundary condition.

Proof. We will give the proof for the discrete conservative quantities of $I_{h,1}$, $I_{h,3}$, $I_{h,4}$ respectively.

Proof for the number of plasmons $I_{h,1}$

Setting the test function $\phi = u$ and $\eta = m$ in the LDG scheme (2.4a) and (2.4b), we get

$$i(u_t, u)_K + \frac{3}{2} < \hat{m}v, u >_{\partial K} - \frac{3}{2}(m, u_x)_K - \frac{1}{2}(uv, u)_K = 0, \tag{2.8}$$

$$(m, m)_K = < \hat{u}v, m >_{\partial K} - (u, m_x)_K. \tag{2.9}$$

Then subtracting the conjugate of (2.8) from (2.8), implies

$$i\frac{d}{dt}(u, u)_K + \frac{3}{2} < \hat{m}v, u >_{\partial K} - \frac{3}{2}(m, u_x)_K - \frac{3}{2} < u, \hat{m}v >_{\partial K} + \frac{3}{2}(u_x, m)_K = 0. \tag{2.10}$$

Similarly, subtracting the conjugate of (2.9) from (2.9) yields

$$0 = < \hat{u}v, m >_{\partial K} - (u, m_x)_K - < m, \hat{u}v >_{\partial K} + (m_x, u)_K. \tag{2.11}$$

Adding (2.10) and $\frac{3}{2} \times$ (2.11), we have

$$i\frac{d}{dt}(u, u)_K + \frac{3}{2}(< \hat{m}v, u >_{\partial K} + < m, \hat{u}v >_{\partial K} - (m, u_x)_K - (m_x, u)_K)$$
$$+ \frac{3}{2}(- < u, \hat{m}v >_{\partial K} - < \hat{u}v, m >_{\partial K} + (u, m_x)_K + (u_x, m)_K) = 0.$$

It is equivalent to

$$i\frac{d}{dt}(u, u)_K + \frac{3}{2}(< \hat{m}v, u >_{\partial K} + < m, \hat{u}v >_{\partial K} - < mv, u >_{\partial K})$$
$$+ \frac{3}{2}(- < u, \hat{m}v >_{\partial K} - < \hat{u}v, m >_{\partial K} + < uv, m >_{\partial K}) = 0,$$

by applying the equalities of $(m, u_x)_K + (m_x, u)_K = < mv, u >_{\partial K}$ and $(u, m_x)_K + (u_x, m)_K = < uv, m >_{\partial K}$. Then summing up for all $K \in \mathcal{T}_h$, it can be shown that

$$\sum_{K \in \mathcal{T}_h} (< \hat{m}v, u >_{\partial K} + < m, \hat{u}v >_{\partial K} - < mv, u >_{\partial K}) = 0, \tag{2.12a}$$

$$\sum_{K \in \mathcal{T}_h} (< u, \hat{m}v >_{\partial K} + < \hat{u}v, m >_{\partial K} - < uv, m >_{\partial K}) = 0, \tag{2.12b}$$

with the choice of numerical fluxes in (2.7a) and the periodic or homogeneous Dirichlet boundary condition, such that

$$i\frac{d}{dt}(u, u)_h = 0.$$

This proves the conservative quantity of $I_{h,1} = const$.

Proof for the energy of the oscillations $I_{h,3}$

To prove the conservative quantity $I_{h,3}$, we first take the time derivative of equation (2.4b) and choose the test function $\eta = m$, to obtain

$$(m_t,m)_K = <\hat{u}_t\boldsymbol{v},m>_{\partial K} - (u_t,m_x)_K, \tag{2.13}$$

and its conjugate

$$(m,m_t)_K = <m,\hat{u}_t\boldsymbol{v}>_{\partial K} - (m_x,u_t)_K. \tag{2.14}$$

Then in (2.4a), we set the test function $\phi = u_t$ to get

$$\mathrm{i}(u_t,u_t)_K + \frac{3}{2}<\hat{m}\boldsymbol{v},u_t>_{\partial K} - \frac{3}{2}(m,u_{tx})_K - \frac{1}{2}(uv,u_t)_K = 0, \tag{2.15}$$

and its conjugate

$$-\mathrm{i}(u_t,u_t)_K + \frac{3}{2}<u_t\boldsymbol{v},\hat{m}>_{\partial K} - \frac{3}{2}(u_{tx},m)_K - \frac{1}{2}(u_t,uv)_K = 0. \tag{2.16}$$

Letting $3\times((2.13)+\times(2.14))-2\times((2.15)+(2.16))$, implies

$$\begin{aligned}
3\frac{d}{dt}(m,m)_K &+ (uv,u_t)_K + (u_t,uv)_K \\
&= 3(<\hat{u}_t\boldsymbol{v},m>_{\partial K} + <u_t\boldsymbol{v},\hat{m}>_{\partial K} - (u_t,m_x)_K - (u_{tx},m)_K) \\
&\quad + 3(<m,\hat{u}_t\boldsymbol{v}>_{\partial K} + <\hat{m}\boldsymbol{v},u_t>_{\partial K} - (m_x,u_t)_K - (m,u_{tx})_K).
\end{aligned}$$

After adding up over $K \in \mathcal{T}_h$ and recalling the equality (2.12), we can see that

$$3\frac{d}{dt}(m,m)_h + (uv,u_t)_h + (u_t,uv)_h = 0. \tag{2.17}$$

In (2.4c), (2.4d) and (2.4e), taking the time derivative of (2.4d) and choosing the test function $\psi = p+q+s, \xi = w$ and $\zeta = v_t$ respectively, implies

$$(v_t,p+q+s)_K + \frac{1}{2}<(\hat{p}+\hat{q}+\hat{s})\boldsymbol{v},p+q+s>_{\partial K} - \frac{1}{2}(p+q+s,(p+q+s)_x)_K = 0, \tag{2.18}$$

$$(w_t,w)_K = <\hat{v}_t\boldsymbol{v},w>_{\partial K} - (v_t,w_x)_K, \tag{2.19}$$

$$(p,v_t)_K = <\hat{w}\boldsymbol{v},v_t>_{\partial K} - (w,v_{tx})_K. \tag{2.20}$$

In (2.5) and (2.6), we choose the test function $\psi = v_t$ to obtain

$$(s,v_t)_K = (|u|^2,v_t)_K, \tag{2.21}$$

$$(q,v_t)_K = (v^2,v_t)_K. \tag{2.22}$$

Combining (2.18)-(2.22), we have

$$(|u|^2,v_t)_K+(v^2,v_t)_K-(w_t,w)_K+[<\hat{v}_t\boldsymbol{\nu},w>_{\partial K}-(v_t,w_x)_K+<\hat{w}\boldsymbol{\nu},v_t>_{\partial K}-(w,v_{tx})_K]$$
$$+\frac{1}{2}<(\hat{p}+\hat{q}+\hat{s})\boldsymbol{\nu},p+q+s>_{\partial K}-\frac{1}{2}(p+q+s,(p+q+s)_x)_K=0.$$

And then summing up for all $K\in\mathcal{T}_h$, implies that

$$(|u|^2,v_t)_h+(v^2,v_t)_h-(w_t,w)_h=0, \tag{2.23}$$

since the similar equality holds for

$$\sum_{K\in\mathcal{T}_h}[<\hat{v}_t\boldsymbol{\nu},w>_{\partial K}-(v_t,w_x)_K+<\hat{w}\boldsymbol{\nu},v_t>_{\partial K}-(w,v_{tx})_K]=0,$$
$$\sum_{K\in\mathcal{T}_h}[<(\hat{p}+\hat{q}+\hat{s})\boldsymbol{\nu},p+q+s>_{\partial K}-(p+q+s,(p+q+s)_x)_K]=0$$

with the numerical fluxes in (2.7a) and the periodic or homogeneous boundary condition. Collecting (2.17) and (2.23), we have proved the discrete conservative quantity $I_{h,3}=const$.

Proof for the number of particles $I_{h,4}$

Choosing the test function $\psi=1$ in the LDG scheme (2.4c) and summing up for all element $K\in\mathcal{T}_h$, we obtain the discrete conservative quantity of the number of particles $I_{h,4}=const$. $\qquad\square$

Remark 2.1. Even though we could not give the second discrete conservative quantity I_2, the numerical fluxes can be determined through the proof of Proposition 2.1. From the numerical tests in the next section, the LDG method works well and all the discrete conservative quantities are preserved very well.

2.5 The LDG method for the integrable system (1.3)

The LDG method can be applied to the integrable system (1.3) by rewriting the system into

$$iu_t+m_x-uv=0, \quad m=u_x,$$
$$v_t+s_x=0, \qquad s=|u|^2.$$

The corresponding LDG scheme is: Find $u,m\in V_h^c,v,w,p,q,s\in V_h^r$, such that

$$i(u_t,\phi)_K+<\hat{m}\boldsymbol{\nu},\phi>_{\partial K}-(m,\phi_x)_K-(uv,\phi)_K=0, \tag{2.24a}$$
$$(m,\eta)_K=<\hat{u}\boldsymbol{\nu},\eta>_{\partial K}-(u,\eta_x)_K, \tag{2.24b}$$
$$(v_t,\psi)_K+<\hat{s}\boldsymbol{\nu},\psi>_{\partial K}-(s,\psi_x)_K=0, \tag{2.24c}$$
$$(s,\xi)_K=(|u|^2,\xi)_K, \tag{2.24d}$$

for all test function $\psi, \eta \in V_h^c$ and $\psi, \xi \in V_h^r$ and for all elements $K \in \mathcal{T}_h$, with the numerical fluxes

$$\hat{s} = \frac{1}{2}(s^- + s^+), \quad \hat{u} = u^-, \quad \hat{m} = m^+. \tag{2.25}$$

Similarly, we can prove the following proposition.

Proposition 2.2. (Discrete conservative quantities) The solutions to the LDG method (2.24) and (2.25) possess the discrete conservative quantities:

- $I_{h,1} = \int |u|^2 dx$,

- $I_{h,3} = \int (|m|^2 + v|u^2|)$,

- $I_{h,4} = \int v dx$,

with periodic or homogeneous Dirichlet boundary condition.

2.6 Time discretization

Now the only thing left is the time discretization. Using the method-of-line, after the spatial discretization is given, we need to choose a stable time discretization for the semi-discrete ODE system (2.4). For example, we can choose an explicit high order Runge-Kutta method with suitable CFL constraint, with the accuracy comparable to the high order DG method. But the CFL constraint for most explicit time discretization method is about $\Delta t \approx h^3$ for the Sch-KdV system (1.2), stemming from the high order spatial derivatives. In this paper, high order semi-implicit methods [17] are employed to relax the CFL constraint to $\Delta t \approx h$, by noticing that in the Sch-KdV system the high order spatial derivatives are all linear. In the semi-implicit methods, the terms containing second and third order spatial derivative will be treated implicitly, and the remaining terms will be treated explicitly. We refer to [17] for more details.

3 Numerical tests

In this section, we present numerical tests of the Sch-KdV system with a solitary wave solution to test the accuracy in Section 2. We also present some soliton-soliton collisions to demonstrate the capability of the method. Semi-implicit time discretization methods are used to increase the efficiency [17]. The stability constraint between the time step Δt and the mesh size h is $\Delta t = \mathcal{O}(h)$. However, we will not address the efficiency of time discretization in this paper. We choose the time step suitably small such that the spatial errors are dominant in the numerical results. With successive mesh refinements, we have verified that all numerical results are mesh convergent.

Example 3.1. Accuracy test: the solitary wave

Sch-KdV system (1.2) admits a stationary traveling localized solution, coupled soliton, given by

$$\begin{cases} u = -\frac{6\sqrt{3}}{5}a\,\text{sech}(\xi)\tanh(\xi)\exp\left\{ia\left[\left(\frac{3}{20}-\frac{a}{6}\right)t-\frac{x}{3}\right]\right\}, \\ v = -\frac{9}{5}\text{sech}^2(\xi), \end{cases} \tag{3.1}$$

where $\xi = \sqrt{(a/10)}(x+at)$ and a is a free positive parameter. Ideally, one would like to solve the system in infinite space. Since all the processes take place in the localized regions of space, we impose the periodic boundary condition for large enough domains. In this example, we choose the domain from -80 to 80. In Fig. 1, the space-time graphs of the stationary traveling localized solutions are shown until $t=50$.
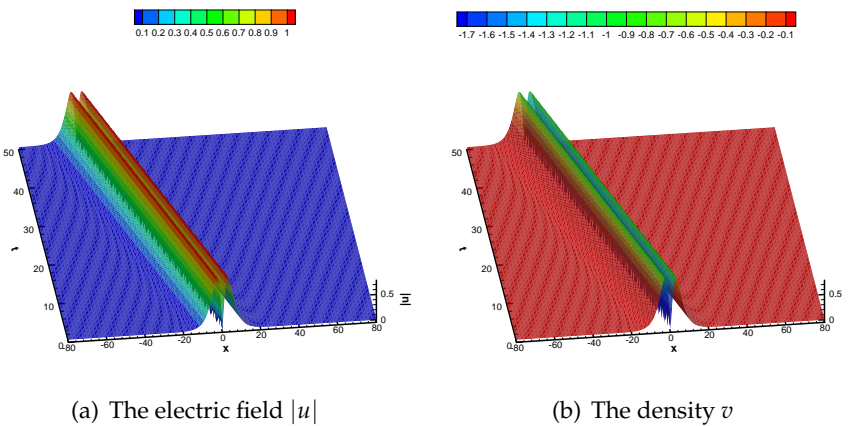

(a) The electric field $|u|$ (b) The density v

Figure 1: The space-time graphs of the stationary traveling localized solutions (3.1) until $t=50$.

Table 1 lists the L^1 errors and orders of $|u|$ and v respectively, at $t=5.0$ on the uniform mesh of different mesh sizes for the piecewise P^1, p^2 and P^3 polynomial bases. It shows that the numerical convergent orders of the LDG scheme are optimal, and thus the LDG method preserves the amplitude, shape and speed of the soliton. In Table 2, we list the L^1 errors of $|u|$ and v respectively, at $t=5.0$ on the uniform mesh of fixed mesh sizes $h=2$, for the piecewise P^k polynomial bases with $k=1,2,\cdots,8$. Spectral orders of LDG method can be found numerically from Table 2. And from Table 1 and 2, we also find the high order LDG scheme has the advantage of using less freedoms than the low order scheme, to gain the same accuracy.

Example 3.2. Accuracy test: the solitary wave for the integrable system (1.3)

The integrable system (1.3) admit the following solitary wave, given by

$$\begin{cases} u = \sqrt{2}\text{sech}(x+t)\exp(i(-x/2+3t/4)), \\ v = -2\text{sech}^2(x+t). \end{cases} \tag{3.2}$$

Table 1: Accuracy test in Example 3.1: L^1 errors and orders of $|u|$ and v, for the solitary solution at time $t=5$ in the domain $[-80,80]$, with piecewise P^k polynomial bases on uniform meshes of different mesh size h.

		$|u|$		v	
	h	L^1 error	order	L^1 error	order
P^1	2	2.11E-02	–	1.74E-02	–
	1	2.70E-03	2.96	1.95E-03	3.16
	1/2	6.13E-04	2.14	4.01E-04	2.28
	1/4	1.50E-04	2.03	9.85E-05	2.03
	1/8	3.73E-05	2.01	2.47E-05	2.00
P^2	2	3.15E-03	–	2.30E-03	–
	1	1.70E-04	4.21	6.77E-05	5.09
	1/2	2.12E-05	3.00	8.08E-06	3.07
	1/4	2.64E-06	3.01	1.00E-06	3.01
	1/8	3.29E-07	3.00	1.25E-07	3.00
P^3	2	3.03E-04	–	1.03E-04	–
	1	1.02E-05	4.89	3.65E-06	4.82
	1/2	6.31E-07	4.01	2.17E-07	4.07
	1/4	3.95E-08	4.00	1.35E-08	4.01
	1/8	2.47E-09	4.00	8.48E-10	3.99

Table 2: Accuracy test in Example 3.1: L^1 errors of $|u|$ and v, for the solitary solution at time $t=5$ in the domain $[-80,80]$, on uniform meshes with mesh size $h=2$ with piecewise P^k polynomial bases, $k=1,2,\cdots,8$.

k	1	2	3	4	5	6	7	8
$|u|$	2.11E-02	3.15E-03	3.03E-04	2.67E-05	3.44E-06	3.60E-07	5.85E-08	5.62E-09
v	1.74E-02	2.30E-03	1.03E-04	3.62E-05	2.32E-06	5.51E-07	4.16E-08	6.95E-09

Since all the processes take place in the localized regions of space, we impose the periodic boundary condition for large enough domains. In this example, we choose the domain from -80 to 80. Table 3 lists the L^1 errors and orders of $|u|$ and v respectively, at $t=5.0$ on the uniform mesh of different mesh sizes for the piecewise P^1, P^2 and P^3 polynomial bases. It shows that the numerical convergent orders of the LDG method for $|u|$ are optimal. For density v, the numerical convergent orders of the LDG scheme are sub-optimal.

Example 3.3. Soliton collisions

In this numerical example we consider the collision of solitons [2]. Piecewise P^3 polynomial bases are used in the LDG method on the uniform mesh with $h=1$. In all the sets of computation, we can observe the similar behavior.

Table 3: Accuracy test in Example 3.2: L^1 errors and orders of $|u|$ and v, for the solitary solution at time $t=5$ in the domain $[-80,80]$, with piecewise P^k polynomial bases on uniform meshes of different mesh size h.

	h	$|u|$		v	
		L^1 error	order	L^1 error	order
P^1	1	1.40E-02	–	2.03E-02	–
	1/2	3.30E-03	2.08	1.15E-02	0.82
	1/4	9.04E-04	1.87	6.13E-03	0.91
	1/8	2.60E-04	1.80	3.11E-03	0.98
	1/16	6.98E-05	1.90	1.56E-03	1.00
P^2	1	1.98E-03	–	9.40E-03	–
	1/2	6.09E-05	5.02	2.02E-03	2.22
	1/4	6.22E-06	3.29	4.43E-04	2.19
	1/8	7.08E-07	3.14	1.05E-04	2.08
	1/16	8.44E-08	3.07	2.60E-05	2.01
P^3	1	1.82E-04	–	1.24E-03	–
	1/2	3.79E-06	5.59	1.67E-04	2.89
	1/4	1.84E-07	4.36	2.25E-05	2.89
	1/8	1.17E-08	3.98	2.88E-06	2.97
	1/16	7.68E-10	3.93	3.62E-07	2.99

Two coupled solitons collision

A typical example is shown in Fig. 2 for the case where two coupled solutions (3.1) with different velocities $a=0.45$ and 0.15. One can see that as soon as the solitons start to overlap the Langmuir field flows out of the density well of the large soliton. Since the effects of the ion dispersion v_{xxx} and nonlinearities v^2 are no longer balanced ponderomotive force $|u|^2$, the density hole of the larger soliton begins to emit sound waves. At the end of the observation time both solitons are broken up into a series of sound trains, positive and negative pulses and the Langmuir wave packets.

Coupled and single solitons collision

Evidently, if $u=0$, the Sch-KdV system has a stationary solution in the form of localized density hump, ion-acoustic single soliton:

$$v=3a\text{sech}^2(\sqrt{a/2}(x-at)). \tag{3.3}$$

We simulate the collision of a coupled soliton (3.1) and a single soliton (3.3). The process proceeds differently for different signs of the total density I_4.

- $I_4 > 0$

  In Fig. 3 we display the course of collision in case when $I_4 > 0$, where the initial parameters for the coupled and single soliton are $a = 0.15$ and 0.3 respectively. It
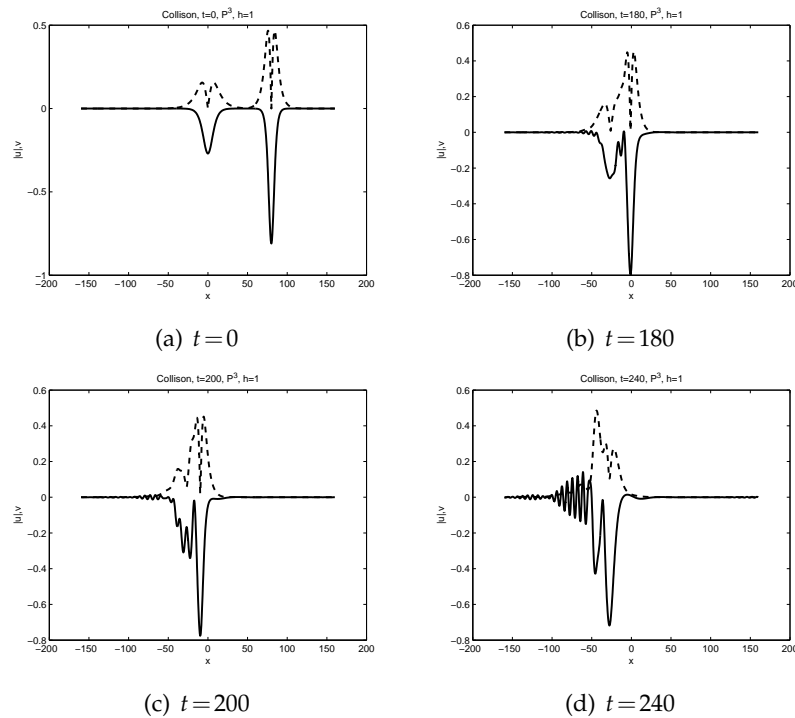
Figure 2: Numerical results of two coupled solitons collision with different velocities $a = 0.45$ and 0.15, solid lines for the density v and the dash line for the electric field $|u|$.

shows that the single soliton passes through the coupled soliton the Langmuir field become untrapped due to the deformation of density well. After the collision, the single soliton reappears and the resulting isolated density hole spreads out into a sound train as in the collision of two coupled solitons.

- $I_4 < 0$

Fig. 4 shows the collision of coupled and single solitons with negative total density I_4. We observe that both coupled and single solitons are destroyed in the collision. These results provide the additional evidence that the dynamic of a coupled soliton are essentially governed by the ion nonlinearities and dispersion in the KdV equation.

Energy conservation

In Fig. 5, we also give the discrete conservative quantities $I_{h,1}$, $I_{h,2}$, $I_{h,3}$, $I_{h,4}$ for the solitons collision results in Figs. 2, 3, 4. We can see that the discrete conservative quantities are preserved very well for the long time simulation until $t = 300$.
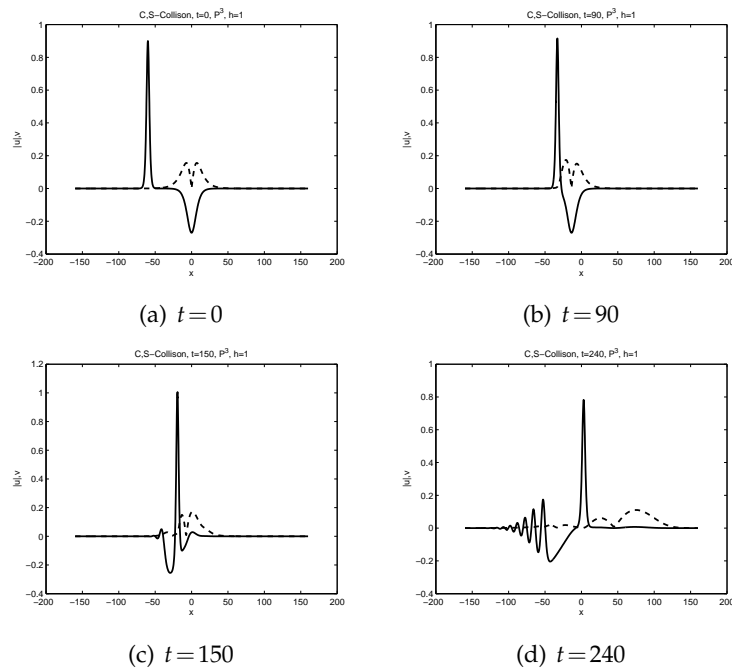
(a) $t=0$

(b) $t=90$

(c) $t=150$

(d) $t=240$

Figure 3: Numerical results of coupled and single solitons collision with different velocities $a=0.15$ and 0.3, with $I_4>0$, solid lines for the density v and the dash line for the electric field $|u|$.
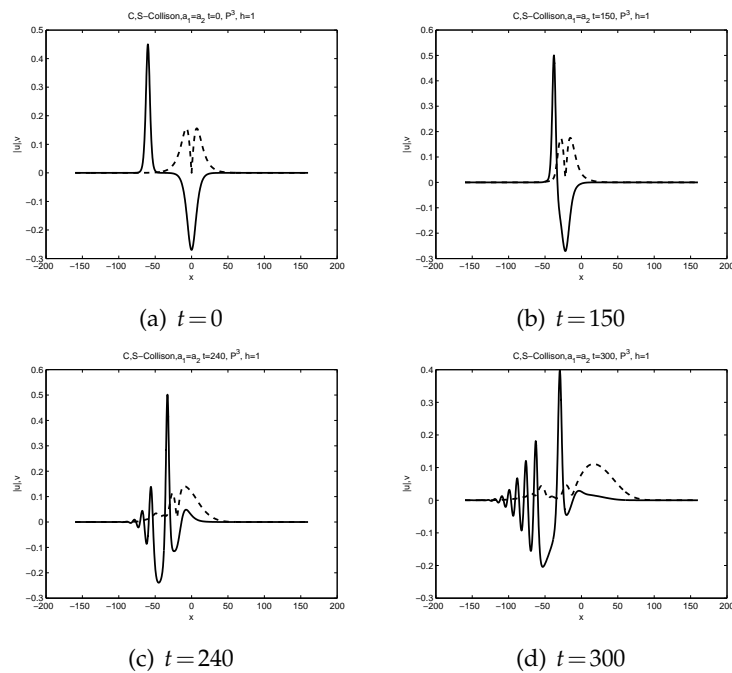

(a) $t=0$

(b) $t=150$

(c) $t=240$

(d) $t=300$

Figure 4: Numerical results of coupled and single solitons collision with velocities $a=0.15$ both, with $I_4<0$, solid lines for the density v and the dash line for the electric field $|u|$.
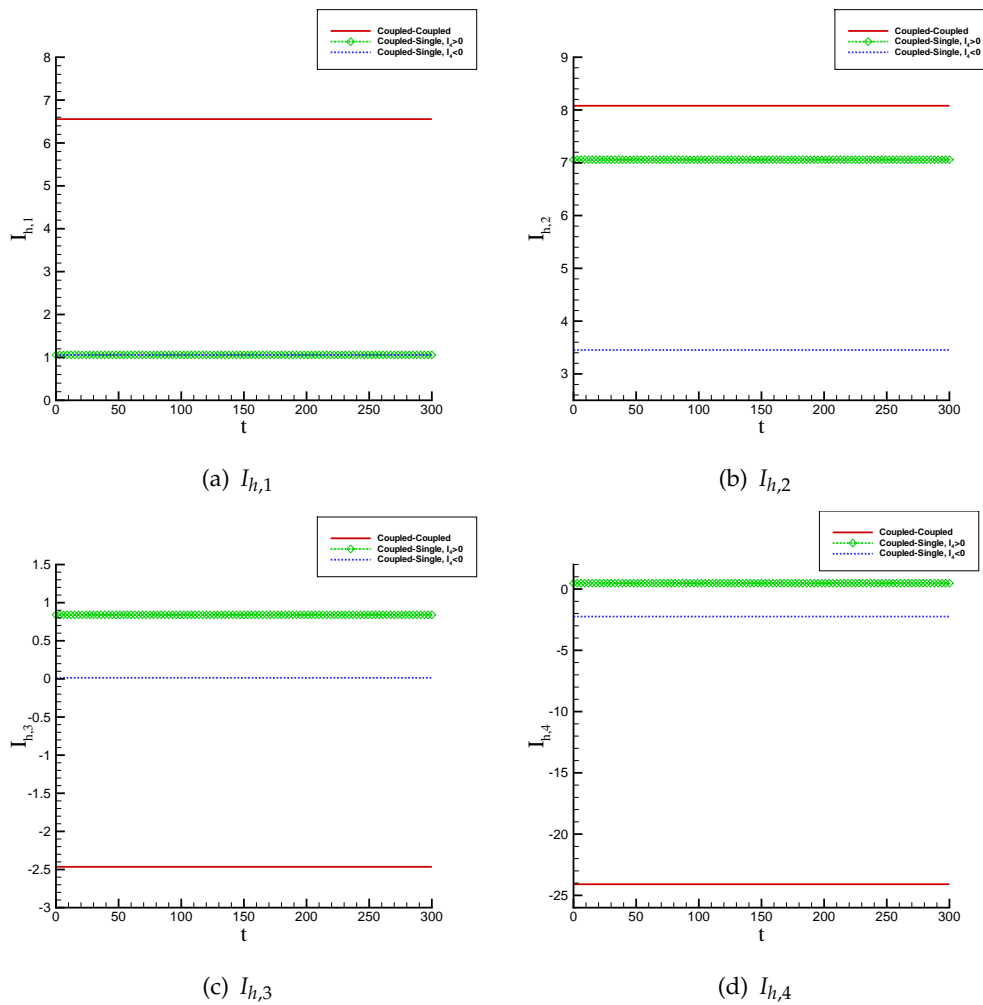
(a) $I_{h,1}$ (b) $I_{h,2}$

(c) $I_{h,3}$ (d) $I_{h,4}$

Figure 5: The discrete conservative quantities $I_{h,1}$, $I_{h,2}$, $I_{h,3}$, $I_{h,4}$ for the solitons collision.

4   Conclusion

In this paper, we construct the conservative LDG method for the Schrödinger-KdV system. We prove that the LDG method conserve the number of plasmons I_1, energy of the oscillations I_3 and the number of particles I_4. High order semi-implicit time discretization is employed to relax the CFL constraint. Numerical tests have been performed to show the numerical optimal accuracy, or sub-optimal accuracy for the density in system (1.3). Some applications of different soliton-soliton collisions have also been performed to show the capability of the LDG method for the Schrödinger-KdV system. The error estimates for the method will give the mechanism of the accuracy order. We leave this topic to our future work.

Acknowledgments

References

[1] J. Albert and J. Angulo Pava, Existence and stability of ground-state solutions of a Schrödinger-KdV system, Proc. Roy. Soc. Edinburgh Sect. A, 133 (2003), 987-1029.
[2] K. Appert and J. Vaclavik, Dynamics of coupled solitons, Phys. Fluids, 20 (1977), 1845-1849.
[3] D.M. Bai and L.M. Zhang, The finite element method for the coupled Schrödinger-KdV equations, Phys. Lett. A, 373 (2009), 2237-2244.
[4] D.M. Bai and L.M. Zhang, Numerical studies on a novel split-step quadratic B-spline finite element method for the coupled Schrödinger-KdV equations, Commun. Nonlinear Sci. Numer. Simul., 16 (2011), 1263-1273.
[5] D.J. Benney, A general theory for interactions between short and long waves, Stud. Appl. Math., 56 (1977), 81-94.
[6] J.L. Bona, H. Chen, O. Karakashian and Y. Xing, Conservative, discontinuous-Galerkin methods for the generalized Korteweg-de Vries equation, Math. Comp., 82(2013), 1401-1432.
[7] B. Cockburn, S. Hou and C.-W. Shu, The Runge-Kutta local projection discontinuous Galerkin finite element method for conservation laws IV: the multidimensional case, Math. Comp., 54 (1990), 545-581.
[8] B. Cockburn, S.-Y. Lin and C.-W. Shu, TVB Runge-Kutta local projection discontinuous Galerkin finite element method for conservation laws III: one dimensional systems, J. Comput. Phys., 84 (1989), 90-113.
[9] B. Cockburn and C.-W. Shu, TVB Runge-Kutta local projection discontinuous Galerkin finite element method for conservation laws II: general framework, Math. Comp., 52 (1989), 411-435.
[10] B. Cockburn and C.-W. Shu, The Runge-Kutta discontinuous Galerkin method for conservation laws V: multidimensional systems, J. Comput. Phys., 141 (1998), 199-224.
[11] B. Cockburn and C.-W. Shu, The local discontinuous Galerkin method for time-dependent convection-diffusion systems, SIAM J. Numer. Anal., 35 (1998), 2440-2463.
[12] A. Golbabai and A. Safdari-Vaighani, A meshless method for numerical solution of the coupled Schrödinger-KdV equations, Computing, 92 (2011), 225-242.
[13] T. Kawahara, N. Sugimoto and T. Kakutani, Nonlinear interaction between short and long capillary-gravity waves, J. Phys. Soc. Japan, 39 (1975), 1379-1386.
[14] V. Makhankov, On stationary solutions of the Schrödinger equation with a self-consistent potential satisfying Boussinesq's equation, Phys. Lett. A, 50 (1974), 42-44.
[15] K. Nishikawa, H. Hojo, K. Mima and H. Ikezi, Coupled nonlinear electron-plasma and ion-acoustic waves, Phys. Rev. Lett., 33 (1974), 148-151.
[16] W.H. Reed and T.R. Hill, Triangular mesh method for the neutron transport equation, Technical report LA-UR-73-479, Los Alamos Scientific Laboratory, Los Alamos, NM, 1973.
[17] Y. Xia, Y. Xu and C.-W. Shu, Efficient time discretization for local discontinuous Galerkin methods, Discrete Contin. Dyn. Syst. Ser. B, 8 (2007), 677-693.

[18] Y. Xia, Y. Xu and C.-W. Shu, Local discontinuous Galerkin methods for the generalized Zakharov system, J. Comput. Phys. 229 (2010), 1238-1259.

[19] Y. Xu and C.-W. Shu, Local discontinuous Galerkin methods for nonlinear Schrodinger equations, J. Comput. Phys., 205 (2005), 72-97.

[20] Y. Xu and C.-W. Shu, Local discontinuous Galerkin methods for high-order time-dependent partial differential equations, Communications in Computational Physics, 7 (2010), 1-46.

[21] N. Yajima and J. Satsuma, Soliton solutions in a diatomic lattice system, Prog. Theor. Phys., 62 (1979), 370-378.

[22] J. Yan and C.-W. Shu, Local discontinuous Galerkin methods for partial differential equations with higher order derivatives, J. Sci. Comput., 17 (2002), 27-47.